Improved correspondence of fMRI visual field localizer data after macroanatomical alignment

Running Title: Visual field localizer & CBA

Qubad M.[1], Barnes-Scheufler C.V.[1], Schaum M.[2], Raspor E.[1], Rösler L.[1,3], Peters B.[4,5], Goebel R.[3,6], Reif A.[1], Bittner R.A.[1,7]*

[1] Department of Psychiatry, Psychosomatic Medicine and Psychotherapy and Brain Imaging Center, University Hospital, Goethe University, Frankfurt, Germany,

[2] Leibniz Institute for Resilience Research, Mainz, Germany

[3] Netherlands Institute for Neuroscience, Amsterdam, The Netherlands

[4] Institute of Medical Psychology, University Hospital, Goethe University, Frankfurt, Germany,

[5] Zuckerman Mind Brain Behavior Institute, Columbia University, New York, NY, USA

[6] Department of Cognitive Neuroscience, Faculty of Psychology and Neuroscience, Maastricht University, Maastricht, The Netherlands

[7] Ernst Strüngmann Institute for Neuroscience (ESI) in Cooperation with Max Planck Society, Frankfurt am Main, Germany

*Corresponding author. Department of Psychiatry, Psychosomatic Medicine and Psychotherapy, University Hospital Frankfurt, Goethe University, Heinrich-Hoffmann-Str. 10, D-60528 Frankfurt am Main, Germany.

Phone: +49 69 6301 84713. Fax: +49 69 6301 81775.

Email: bittner@med.uni-frankfurt.de

Total number of words in abstract: 200/200

Total number of words in main text: 3444/4500

29 **ORCID IDs**

30 M.Q.: orcid.org/0000-0002-9291-5739

31 C.V.B.-S.: orcid.org/0000-0002-4730-1981

32 M.S.: orcid.org/0000-0002-6589-4530

33 E.R.: orcid.org/0000-0003-4418-7084

34 L.R.: orcid.org/0000-0003-1046-1073

35 B.P.: orcid.org/0000-0002-0948-8976

36 R.G.: orcid.org/0000-0003-1780-2467

37 A.R.: orcid.org/0000-0002-0992-634X

38 R.A.B.: orcid.org/0000-0003-2021-0358

ABSTRACT

The study of the visual system and its role for human cognition with fMRI often requires the use of localizer paradigms to define regions of interest (ROIs). However, the considerable degree of interindividual variability of the cerebral cortex represents an important confound, when analyzing data on the group level. Cortex-based alignment (CBA) techniques lead to a reliable reduction of interindividual macroanatomical variability. Yet, CBA has not been evaluated for visual field localizer paradigms used to map specific parts of the visual field within retinotopically organized early visual areas. We evaluated CBA for an attention-enhanced visual field localizer mapping a homologous part of each visual quadrant in 50 participants. After CBA, group ROIs showed markedly increased spatial consistency. CBA also led to an increase in the probability of activation overlap of up to forty percent. Furthermore, after CBA group ROI size for the lower visual hemifield was larger than for the upper. This asymmetry, which mirrors previous mapping studies, was not detectable before CBA. Our results confirm and extend the utility of CBA for the study of the visual system in the context of group analyses. CBA should be particularly relevant when studying neuropsychiatric disorders with abnormally increased interindividual macroanatomical variability.

KEYWORDS

Human visual cortex, fMRI, visual-field localizer, cortex-based alignment

INTRODUCTION

The visual system includes a multitude of topographical representations of varying resolution across increasingly specialized[1] visual areas. Functional magnetic resonance imaging (fMRI) offers a variety of methods either to map these topographical representations in full, or to localize specific visual areas or retinotopic positions within their topography. These approaches are essential not only for the fine-grained study of fundamental properties of the visual system[1], but also for investigating the role of these areas for higher-order cognitive processes such as visual attention and working memory[2-6]. This also extends to translational studies of visual dysfunction and its cognitive consequences in neuropsychiatric disorders[7,8].

Methods for fMRI-based visual mapping, i.e. techniques to define regions of interest in the visual system based on specific functional properties, fall in in three broad categories: retinotopic mapping, visual field localizer and functional localizer paradigms. Retinotopic mapping and the more advanced population receptive field mapping allow the complete delineation of early visual areas[1,9,10]. Conversely, visual field localizer paradigms can map a circumscribed region within a retinotopically organized visual area[11,12]. Finally, functional localizers can detect higher-order visual areas such as the fusiform face area, parahippocampal place area (PPA), extrastriate body area (EBA), lateral occipital complex (LOC), which are clustered and show specialization for the processing of specific categories of complex visual information[1,13,14]. In most fMRI studies, high interindividual anatomical variability of cortical areas in terms of both size and location constitutes an important challenge[15-23]. For instance, it has been shown that primary visual cortex (V1) can differ in size by about 2-fold between individuals[17]. Furthermore, anatomical variability in terms of location has been shown to be particularly pronounced in extrastriate visual areas[24]. This crucial confound reduces the power to reliably map visual areas at the group level.

One way to mitigate this problem for the visual system is to pool single-subject ROIs, while simultaneously using the overall group-based probability for that ROI at each point in a Cartesian coordinate system as a constraint[25-27]. While such a single-subject-based analysis improves sensitivity and functional resolution compared to a standard group-based approach, it

does not actually reduce macroanatomical variability. Additionally, studying the interplay between visual areas and other cortical areas more directly involved in higher-order cognitive processes with whole-brain methods such as functional connectomics network analyses[28] might preclude a single-subject based strategy.

Such group-based analyses typically require spatial normalization of structural and functional imaging data to a common Cartesian coordinate system such as Talairach[29] or MNI[30] space. In its most basic form, volume-based spatial normalization employs a linear transformation that matches the overall extents of the brains to a standard brain template. While transformation into Talairach space relies on anatomical landmarks, transformation into MNI space utilizes fully data driven registration of structural images to an average template brain[30]. While these spatial normalization approaches inherently lead to an alignment of brains, the underlying algorithms are not specifically geared toward aligning homologous brain structures. Conversely, more refined methods employ non-linear warping algorithms guided by intensity differences to improve macroanatomical alignment[31]. Thus, all of these methods can be categorized as volume-based alignment (VBA) techniques.

However, both linear and nonlinear VBA mostly disregard the topological properties of the cerebral cortex and its geometric features such as sulci and gyri. Consequently, VBA methods result in a considerable amount of residual inter-subject anatomical variability[32,33]. Surface-based procedures constitute an important alternative approach. Surface-based normalization typically uses a geodesic coordinate system, which allows for a two-dimensional representation of the cerebral cortex and respects the cortical topography to a much larger degree than a traditional Cartesian coordinate system[18,34]. Surface-based spatial normalization allows to constrain data preprocessing such as spatial smoothing to cortical tissue, greatly reducing signal contamination by white matter and cerebrospinal fluid. Another advantage of surface-based spatial normalization is the possibility to use individual cortical folding patterns for an additional fully data-driven macroanatomical alignment. Compared to VBA techniques, these cortex-based alignment (CBA) methods considerably improve anatomical correspondence of cortical structures thus leading to a notable reduction of residual inter-

subject anatomical variability[18,34-37]. CBA has also been shown to correctly align cyto-architectonic boundaries[38].

Due to these properties CBA methods have been proposed as an alternative approach specifically for the visual system[26]. Several studies have compared the impact of VBA and CBA methods on specific visual mapping techniques. For retinotopic mapping an improvement of functional overlap in both V1 and V2 after CBA has been demonstrated[34,39]. Furthermore, for functional localizer data CBA substantially increases the overlap of object processing areas LOC, FFA and PPA across subjects[19,40-42]. Conversely, the effects of CBA on visual field localizer paradigms mapping specific retinotopic positions have not been studied. Thus, the utility of CBA has been demonstrated for two of the three main categories of visual mapping methods, i.e. those methods, which map whole areas, either defined by cytoarchitectonic (e.g. V1) or functional (e.g. FFA) properties. Conversely, it remains unclear, to which degree CBA can improve the alignment of ROIs mapped by visual field localizer paradigms. Such paradigms are required for the detailed study of the local processing of simple visual stimuli in early visual areas[11,12,43-45]. Flashing chequerboards covering the exact area of interest within the visual field are primarily used for this purpose. Chequerboards lead to a particularly strong BOLD-signal increase in early visual areas (V1-V3)[46]. To maximize the fidelity of the resulting localizer maps, visual field localizer paradigms typically utilize the fact that attentional modulation induced by task demands significantly enhances response reliability across visual areas. This can be accomplished by adding a simple target detection task[47].

We used such an attention-enhanced visual field localizer paradigm to map a circumscribed location in each visual quadrant across early visual areas in order to define ROIs to be used for the study of higher cognitive processes. We chose a CBA method using a dynamic group average as the target brain[19]. Thus, we eliminated the possible confound of a static CBA target based on an individual brain, whose cortical folding pattern might by chance deviate considerably from the group average.

Our primary goal was to examine the effects of CBA for a visual field localizer paradigm. More specifically, we aimed to determine, whether CBA can improve the reliability of mapping subregions within retinotopically organized visual areas delineated by such a paradigm at the group level. Based on previous findings for other localizer paradigm classes and the relatively good structural-functional correspondence in posterior occipital cortex, we expected to observe a benefit of CBA when aligning subregions within early visual cortex.

Additionally, we compared two methods for the definition of single subject ROIs: the use of extended peak vertices, i.e. single vertices showing the strongest level of activation in a certain brain region and their immediately surrounding vertices, and the delineation of a larger ROI, which includes all vertices above a prespecified threshold, which is kept constant across brain regions[48]. Our goal was to compare these two approaches and to assess changes in spatial correspondence after CBA at the single subject level. Mirroring our hypotheses for the group analyses, we expected to observe an improved correspondence of single-subject peak-vertex ROIs after CBA.

Interestingly, several studies have shown differential response properties such as receptive field size for homologous early visual areas by visual quadrant or hemifield. For instance, improved behavioral performance and higher BOLD-signal amplitudes were observed in the lower visual hemifield[49-52]. We were therefore also interested, whether we could observe differences between upper and lower visual hemifields in our group analysis after CBA. Overall, the aim of the study was to close an important gap in the evaluation of CBA for the study of the visual system. Since visual field localizers are crucial for investigating the contribution of the visual system to higher-order cognitive processes, our results should have implications for the study of visual cognition in both for basic and translational research.

RESULTS

<u>Impact of CBA on spatial consistency of ROIs (group level)</u>

Group-level mapping of the four visual quadrants revealed considerable differences before and after CBA. For the right lower visual quadrant, our analysis before CBA yielded a large

cluster in the left upper occipital cortex, also encompassing posterior parts of temporal cortex, which decreased considerably in size after CBA and was much more circumscribed. Conversely, for the other three visual quadrants, our analysis before CBA yielded clusters in the corresponding parts of the occipital pole, which increased in size after CBA without a notable change of their center of gravity (Figure 2, Table 1). Overall, after CBA group ROIs showed markedly greater spatial consistency and vertical symmetry. Additionally, after CBA, ROIs for the lower visual hemifield were considerably larger in size than ROIs for the upper visual hemifield. Before and after CBA, average time courses showed clear position selectivity which increased after CBA (Figure 2).

Probability maps (group level)

Before CBA, probability maps showed a relatively wide spread of functional activation around the core region of interest defined in our previous group analysis (Figure 3). Here, the maximum probability of overlap of around 50 % was consistently located at the center of each ROI. After CBA, probability maps showed a noticeable decrease in the spread of functional activation around the core region of interest with a corresponding increase in the maximum probability of overlap. Consequently, probability difference maps (Figure 4) showed an increase in the probability of overlap of up to 40 % around the core region of interest and a corresponding peripheral decrease in the probability of overlap of up to 40 %.

Comparison of full ROIs and extended peak-vertex ROIs (single-subject level)

The comparison of time courses averaged over all full single subject ROIs with time courses averaged over all single subject extended peak-vertex ROIs showed consistently larger BOLD signal amplitudes for extended peak-vertex ROIs (Figure 5). There was no difference in BOLD signal amplitude before and after CBA for both types of ROI. Before and after CBA, all ROIs showed comparable clear position selectivity.

The rate of success for finding a ROI for each subject was as follows: upper right visual quadrant 46 out of 50 subjects, upper left visual quadrant 50 out of 50 subjects, lower left visual quadrant 48 out of 50 subjects, lower right visual quadrant 50 out of 50 subjects.

Impact of CBA on spatial variability of peak vertex distribution (single-subject level)

As with the probability maps at the group level, peak vertex distribution maps at the single-subject level (Figure 6) showed less spatial variability after CBA with an increased probability of overlap. Both before and after CBA, the spread of peak vertices was larger for the lower visual quadrants.

DISCUSSION

The aim of our study was to evaluate the utility of CBA for an attention-enhanced visual field localizer paradigm used to map a circumscribed region within retinotopically organized visual areas. Our paradigm mapped homologous regions in each visual quadrant reliably across early visual areas. As expected, CBA led to a marked reduction in macroanatomical variability. On the functional level, CBA had a number of beneficial effects.

CBA improved the results of the group ROI analysis for all visual quadrants (Figure 2). This was reflected in both the spatial consistency of the resulting group ROIs and in the signal-to-noise ratio exemplified by the difference between the BOLD signal amplitude for the stimulated location compared to the other locations. Probability difference maps showed an increase in the probability of overlap of up to forty percent in the central region of interest, which resulted in considerably more focused activation patterns. However, the opposite effect was observed in more peripheral vertices (Figure 4). The latter effect is most likely not attributable to a decrease of spatial overlap in the periphery of early visual areas. Rather it demonstrates that CBA consistently reduces spurious spread-out activation resulting from poor macroanatomical correspondence after VBA. This observation suggests that volume-based group analyses generally overestimate the extent of visual areas. Together these find-

228 ings indicate that CBA substantially increases statistical power when studying early visual ar-
229 eas at the group level. Naturally, this effect of CBA also extends to studies with a more global
230 focus, such as connectivity analyses[53,54].
231 Regarding the comparison between full single-subject ROIs and extended peak-vertex sin-
232 gle-subject ROIs, we made the following observations. As expected, BOLD signal amplitudes
233 for single subject ROIs were not affected by CBA (Figure 5). Conversely, the variability of
234 these ROIs as signified by the peak vertex location decreased after CBA (Figure 6). This un-
235 derscores that the reduction of functional inter-subject variability due to CBA is the main rea-
236 son for our improved results at the group level. Furthermore, BOLD signal amplitudes for the
237 full single-subject ROIs were consistently lower compared to our extended single-subject
238 peak vertex ROIs (Figure 5). This is well in line with previous findings in volume space of
239 larger effect sizes for ROI definition strategies using peak-voxels with or without including di-
240 rectly neighboring voxels[48].
241 Before CBA we observed the strongest group effects, i.e. the largest group ROIs, for the left
242 upper and right lower visual quadrant, an effect that clearly did not persist after CBA (Figure
243 2). Notably, several studies using volume-based fMRI and magnetoencephalographic anal-
244 yses reported lateralized effects on neurophysiological parameters in early visual areas [55,56].
245 Our observation raises the question, whether these findings could at least partly be explained
246 by lateralized differences in macro-anatomical variability rather than true functional differ-
247 ences.
248 Conversely, our CBA-aided group analysis allowed us to compare the response properties of
249 each visual quadrant in a more unbiased way. We observed larger group ROIs for the lower
250 visual hemifield. In a CBA-based probabilistic atlas of the visual system, which included all
251 regions that could be defined in more than 50% of subjects, probabilistic ROIs for dorsal V1
252 and V2 were also noticeably larger than probability maps for ventral V1 and V2, whereas this
253 effect was less clear for V3[41]. These results are in line with our own findings and could be at-
254 tributable to higher residual anatomical variability after CBA in ventral occipital cortex repre-

senting the upper visual hemifield. Alternatively, they could be due to true differences in response properties such as receptive field size or overall area size. The latter interpretation is supported by studies showing functional differences between upper and lower visual hemifields already at the retinal level in the form of differences in receptor densities. Cone density was higher in the superior parts of the retina which processes information from lower visual fields. Conversely, higher rod density was observed in the inferior parts[57,58]. Moreover, Eickhoff et al. observed dorso-ventral asymmetries in receptor densities in V2 and V3[57]. They found a higher density of GABA-A, benzodiazepine- as well as muscarinic M3-receptors in ventral parts of V2 and V3. Furthermore, there is evidence for fundamental differences in receptive field shape from a pRF mapping study. Estimating both the aspect ratios and the size of the mapped areas, a more elliptical receptive field shape was observed for the upper visual hemifield represented by ventral parts of the visual cortex being compared to the lower visual hemifield represented by dorsal parts of the visual cortex[59]. Additionally, there is evidence for a behavioral advantage in the lower visual hemifield for shape discrimination as well as higher BOLD-signal changes and peak amplitudes of MEG/EEG responses[49,51,52,60,61]. Together, these findings demonstrate clear differences in the functional architecture of early visual areas representing the upper and lower visual hemifield. This has been attributed to the fact that the lower visual hemifield represented by dorsal parts of the occipital lobe is more closely linked to the dorsal visual pathway, while the upper visual hemifield represented by ventral parts of the occipital lobe is more closely linked to the ventral visual pathway[62,63]. Furthermore, there is evidence for fundamental differences in receptive field shape from a pRF mapping study. For the upper visual hemifield represented by ventral parts of the visual cortex an increased size and more elliptical shape of receptive fields was observed compared to the lower visual hemifield represented by dorsal parts of the visual cortex[59]. This implies, that the lower visual field is more specialized for the precise localization and representation of space. Our observation of larger ROIs in the lower visual hemifield is in line with these findings. Thus, our results imply that CBA is a useful tool to extend the study of functional and behavioral asymmetries in early visual areas to the group level.

One important limitation of the current study is the lack of a complementary retinotopic mapping data set due to time constraints. This data would have allowed us to delineate the boundaries of early visual areas and pinpoint the exact visual area containing each individual single-subject ROI. Retinotopic mapping studies indicate that peak activation of single subjects assessed by visual localizers are not consistently located in the same visual area. Most localizer tasks show peak activation not in V1 but rather in V2 or V3[12]. It is therefore very likely that our single-subject peak activation did not consistently belong to the same visual cortical area. With the current data set we cannot determine how precisely individual visual areas were aligned with CBA, and whether individual levels of the visual cortical hierarchy were differentially affected. However, the position of our group regions of interest, which bordered the calcarine sulcus and spanned the occipital pole, indicate that they mainly comprised V2 and V3. Similarly, after CBA a comparable increase in the probability of overlap was observed in the same part of occipital cortex. While this is at least suggestive of a relatively consistent benefit of CBA across visual areas, more fine-grained studies including retinotopic mapping are required to definitively address this question.

Furthermore, we did not use eye tracking to insure sufficient fixation. We also did not include an additional central attentional control task on the fixation cross, which would have further encouraged continuous fixation. This was done deliberately in order to keep the difficulty level adequate for psychiatric patient populations, but it might explain our failure to find reliable activation in early visual areas in a fraction of our subjects.

Our study also has implications beyond mapping the visual system in healthy populations. Visual processing deficits are a prominent feature of neurodevelopmental psychiatric disorders such as ADHD, schizophrenia and autism spectrum disorders[7,8,64-71], which can also perturb crucial higher order cognitive processes including working memory[72-74]. The current localizer paradigm will be useful to investigate local impairments of visual information processing as well as disturbances in the interplay between early visual areas and brain networks supporting higher-order cognitive processes. Here, CBA will be particularly relevant to reduce the confounding effects of increased macroanatomical variability in disorders such as

schizophrenia in order to detect true group differences and true functional variability[35,75]. On the other hand, CBA should also be crucial for investigating the neurodevelopmental underpinnings of increased macroanatomical variability itself. To this end the inclusion of probabilistic atlases containing information about gene expression profiles[76] as well as cyto- and receptor architectonics[77,78] will be valuable.

Our CBA approach relied solely on cortical curvature information to reduce macroanatomical variability. The advantage of this method is its feasibility for the vast majority of fMRI data sets, since it only requires a structural brain scan of sufficient quality. Among comparable methods it is the most data driven and objective approach. However, the achievable reduction of macroanatomical variability is limited by the variable and imperfect correlation between brain structure and brain function[34,37]. Therefore, more advanced methods additionally utilize orthogonal functional data to further reduce anatomical variability. This includes the use of activation patterns or functional connectivity patterns to improve macroanatomical alignment across the whole brain[20,79,80]. Furthermore, a more complex approach has been proposed, which aligns cortical data using ‘areal features’ more closely tied to cortical areas than cortical folding patterns, including maps of relative myelin content and functional resting state networks[81]. These methods have shown to provide a relevant additional reduction of macroanatomical variability for a variety of paradigms including visual functional localizers. Future studies should also evaluate these methods for retinotopic mapping and visual field localizers. Moreover, it has been demonstrated for early auditory areas, that the additional use of a probabilistic atlas of cytoarchitectonically defined areas further improves standard CBA results[82]. Such an approach would easily be feasible for the visual system.

To summarize, we demonstrated the clear superiority of CBA compared to VBA for the analysis of visual field localizer data on the group level indicated by a forty percent increase of overlap of ROIs. Our findings extend previous studies examining other major categories of visual mapping techniques. They underscore the comparable loss of information and statistical power incurred by the use of VBA methods in the majority of fMRI studies. Therefore,

CBA and other comparable methods should be seriously considered as a standard procedure for the detailed study of visual information processing and its disturbance in mental disorders.

METHODS AND MATERIALS

Participants:

All participants gave their written consent to participate in the study. The ethical review board of the Faculty of Medicine at Goethe University granted ethic approval. We recruited 51 healthy volunteers (male : female = 23 : 28) with age ranging between 18-43 years (mean = 24). All participants were non-smokers, had no history of neurological or psychiatric illness and reported normal or corrected-to-normal visual acuity. One participant was left-handed as assessed by the German version of the Edinburgh Handedness Inventory[83].

Stimuli and task:

Subjects performed a visual field localizer paradigm (Figure 1) implemented using Presentation® (Neurobehavioral Systems, Version 18.0) as part of a larger study investigating the role of visual areas for higher cognitive functions. The task consisted of a series of flickering black-and-white-colored round shaped chequerboard stimuli (flicker frequency = 7.5 Hz). Chequerboard stimuli appeared for 2000 ms randomly at one of four different locations (non-target trial). Each location mapped a homologous position in one of the four visual quadrants. Our paradigm featured a simple target-detection task. During thirty-six trials, the two centrally located squares of the chequerboard changed their color to yellow for 133 ms (target trial). Participants were instructed to press a response box button with their left thumb as quickly as possible if they detected a target. The task consisted of a total of 144 trials (36 target trials, 108 standard trials). Thus, target probability was 25 %. The regular inter-stimulus interval was 0 ms. However, once every 10 to 14 trials the inter-stimulus interval increased to 2000 ms. Throughout the task a black, x-shaped fixation cross was displayed at the center of the

screen. Participants were instructed to continuously fixate on the fixation cross. Before the first trial, only the fixation cross was displayed for 10 seconds. After the last trial, only the fixation cross was displayed for 20 seconds. The total duration of the paradigm was 340 seconds. For the purpose of our analyses we defined a total of four conditions, one for each of the four stimulus locations. Each participant practiced the task prior to the measurement.

Acquisition and analysis of fMRI data:

We acquired functional MRI data on a Siemens 3T MAGNETOM Trio scanner at the Goethe University Brain Imaging Centre using a gradient-echo 2D EPI sequence (32 axial slices, TR = 2000 ms, TE = 30 ms, FA = 90°, FoV = 192 x 192 mm2, voxel size = 3 x 3 x 3 mm^3, gap = 1 mm, effective slice thickness = 4 mm). Slices were positioned parallel to the anterior- and posterior commissure. Functional images were acquired in a single run comprising the acquisition of 170 volumes. Immediately before each functional run, 6 volumes of this 2D EPI sequence were acquired with identical parameters except for a switch of phase encoding direction (posterior to anterior instead of anterior to posterior) for EPI distortion correction. Anatomical MRI data for cortex reconstruction and co-registration with functional MRI data was acquired with a high-resolution T1-weighted 3D volume using a Magnetization-Prepared Rapid Gradient-Echo (MP-RAGE) sequence (192 sagittal slices, TR = 1900 ms, TE = 3.04 ms, TI 900 ms, FA = 9°, FoV = 256 x 256 mm^2, voxel size = 1 x 1 x 1 mm^3). Stimulus presentation was constantly synchronized with the fMRI sequence. Head motion was minimized with pillows. The task was projected by a beamer onto a mirror attached on the head coil. MRI data were pre-processed and analyzed using Brain Voyager 20.6[84], the NeuroElf Matlab toolbox (www.neuroelf.net) and custom software written in Matlab. One subject had to be excluded due to excessive intra-scan motion.

Structural image pre-processing:

Structural data pre-processing included background cleaning, brain extraction and bias field correction to minimize image intensity inhomogeneities[84]. Bias field correction employed a "surface fitting" approach using singular value decomposition based least squares low-order

394 (Legendre) polynomials to model low-frequency variations across 3D image space[85]. We
395 used polynomials with an order of 3, which were fitted to a subset of voxels labeled as be-
396 longing to white matter. The estimated parameters of the polynomials were used to construct
397 a bias field which was removed from the data. Our approach comprised of one iteration using
398 automatic white matter labeling[86] and four iterations using manual white matter labeling.
399 Subsequently, structural data were transformed into Talairach coordinate space[29]. This com-
400 prised manual labeling the anterior commissure (AC) and posterior commissure (PC) as well
401 as the borders of the cerebrum. These landmarks were then used to rotate each brain in the
402 AC–PC plane followed by piece-wise, linear transformations to fit each brain in the common
403 Talairach "proportional grid" system[19]. Transformation into Talairach coordinate space was
404 performed because the subsequent automatic segmentation procedure exploits anatomical
405 knowledge for initial brain segmentation including removing subcortical structures and dis-
406 connection of cortical hemispheres. To prepare the data for this procedure, we performed a
407 manual filling of the lateral ventricles. Based on the automatic segmentation of the structural
408 scans along the white–grey matter boundary[87], cortical hemispheres were reconstructed into
409 folded, topologically correct mesh representations, which were tessellated to produce surface
410 reconstructions and calculate curvature maps reflecting the individual cortical folding pat-
411 terns. Surface reconstructions were subsequently morphed into distortion corrected spherical
412 representations.
413
414 <u>Cortex-based alignment of structural data:</u>
415 We then applied for each hemisphere separately a high-resolution, multiscale cortex-based
416 alignment procedure based on the individual curvature maps of all 50 participants. This CBA
417 approach, which reliably aligns corresponding gyri and sulci across subjects[84], consists of an
418 initial rigid and a subsequent non-rigid alignment step[19]. Non-rigid CBA employs a coarse-to-
419 fine matching strategy. Initially, curvature maps contain only smoothed versions of major an-
420 atomical landmarks, adding increasingly more anatomical detail until all curvature information

from each hemisphere is included. It aligns each cortical folding pattern to a dynamically updated group average through iterative morphing. This moving target approach, which generates the target curvature map from the average curvature across all hemispheres at a given alignment stage avoids the possible confounding effects of a suboptimal selection of an individual target brain, whose folding pattern might deviate considerably from the cohort average.

We first conducted a preliminary CBA encompassing both steps to generate an aligned average brain, which we used for a second, final CBA. During the initial step, we aligned the cortical folding pattern of each sphere rigidly to the cortical folding pattern of a randomly selected target sphere by global rotation. We used the rotation parameters with the highest degree of overlap between the curvature of each individual sphere and the target sphere as the starting point for the subsequent preliminary non-rigid CBA. The results of this preliminary non-rigid CBA procedure were only used to generate an average brain to be used as an unbiased target for the final rigid alignment step. This procedure allowed us to minimize the influence of a suboptimal target brain during the rigid alignment step. The resulting optimal rotation parameters were used as the starting point for the subsequent final non-rigid CBA. After the final non-rigid CBA, we merged both hemispheres of each individual brain to create a global surface-based analysis space.

Furthermore, we created average hemispheres from the original folded mesh representations, which were subsequently merged, inflated and used for data analysis and visualization. Averaging of hemispheres was repeated after applying the transformation matrix of the final rigid and non-rigid CBA to the folded mesh representations, resulting in an accurate representation of the effects of macroanatomical alignment.

<u>Functional image pre-processing:</u>

Initial volume-based pre-processing of functional MRI data comprised slice timing correction using sinc interpolation and 3D motion correction using sinc interpolation. Next, we performed echo-planar imaging distortion correction using the Correction based on Opposite

449 Phase Encoding (COPE) method[88]. The EPI distortion corrected functional data were co-reg-
450 istered to the untransformed extracted brains utilizing a boundary-based registration algo-
451 rithm optimized for the use in surface-based analyses[89]. After co-registration to volume
452 space, functional data were transformed into Talairach coordinate space using the transfor-
453 mation matrix generated during Talairach transformation of the anatomical data. The volu-
454 metric functional data were then transformed into surface space by sampling on the individ-
455 ual cortical surface incorporating data from −1 to +3 mm along vertex normals. Subsequent
456 pre-processing of functional MRI data in surface space comprised spatial smoothing using a
457 nearest neighbor interpolation (1 iteration, approximating a 2D Gaussian smoothing kernel
458 with a FWHM of 1 mm), linear trend removal and temporal high-pass filtering (high-pass
459 0.00903 Hz). Spatial smoothing in surface space is clearly superior to spatial smoothing in
460 volume space by avoiding contamination from cortical areas proximal in volume space but
461 more distant in surface space[19,53]. However, we still opted for minimum spatial smoothing to
462 prevent a loss of accuracy for our visual field localizer. Based on the vertex-to-vertex refer-
463 encing from the folded, topologically correct meshes to the spherical representations, we
464 mapped the fully preprocessed functional data into a common spherical coordinate system.
465 Finally, we applied surface-based anatomical masks that only included cortical vertices in our
466 analysis to the functional data. These masks excluded those subcortical structures, i.e. parts
467 of thalamus and the basal ganglia, which mapped onto the midline of our surface reconstruc-
468 tions.
469
470 <u>fMRI group analysis:</u>
471 We performed multi-subject statistical analyses using multiple linear regression of the BOLD
472 signal. The presentation of each chequerboard stimulus sequence at a single location, was
473 modelled by an ideal box-car function, which covered the volume of each trial, convolved
474 with a synthetic two-gamma function. These predictors were used to build the design matrix
475 of the experiment. Individual statistical maps were generated by associating each voxel with
476 the beta-value corresponding to the specific set of predictors and calculated on the basis of

the least mean squares solution of the general linear model. The resulting individual statistical maps were entered into a second-level random-effects group analysis using a summary statistic approach.

To study the effects of surface-based macroanatomical alignment, we computed the same analysis steps in surface space before and after CBA, following the protocol established by previous works evaluating this particular method[19,90]. Thus, we essentially compared the impact of pure surface-based registration, referred to as “pre-CBA”, with explicit surface-based macroanatomical alignment, referred to as “post-CBA”. However, for the purpose of our study, we consider the former (pre-CBA) to be a good proxy for VBA, while allowing to directly contrast its results with those of our post-CBA analysis within the same coordinate system.

<u>Group analysis of visual quadrants before and after CBA:</u>

We performed analyses focusing on the mapping of the four visual quadrants at the group level and compared these with results at single subject level. To define the group level ROI for each visual quadrant, we computed separate weighted contrasts for each quadrant against the other three quadrants. We assigned a weight of three to the position of interest, e.g. $(\beta^{Quad1} \times 3) / (\beta^{Quad2} + \beta^{Quad3} + \beta^{Quad4})$ ($p < 0.5$, Bonferroni corrected). For each resulting group level ROI, we extracted average time courses (incl. standard errors of the mean = SEM) for all four conditions. We conducted this analysis both before and after CBA.

<u>Probability maps before and after CBA:</u>

To quantify and visualize variability of functional activation and possible changes due to macroanatomical alignment, the use of probability maps has been proposed. Probability maps are specifically useful to quantify inconsistency i.e. the disparity between individuals regarding the location of a particular (visual) area. To quantify the spatial consistency of activation patterns before and after CBA, we generated probability maps for each visual quad-

rant [91,92]. These maps represent the relative number of subjects showing significant task activity in our single-subject analysis. Probability maps for early visual areas before and after CBA were created based on the previously generated single subject t-maps, with a threshold of a minimum of ten percent probability. To quantify the change in spatial consistency of activation patterns as a result of CBA, we created probability difference maps for each position (post-CBA minus pre-CBA). This allowed us to determine both increases and decreases of spatial consistency due to CBA.

Single-subject ROIs of visual quadrants before and after CBA including peak vertex mapping:

For analyses at single-subject level, we first defined ROIs for each subject independently using the same weighted contrasts employed in the group analysis. We applied a more lenient statistical threshold ($p < 0.05$ uncorrected). For each resulting single-subject ROI we extracted average time courses for all four conditions. We then averaged these time courses across all subjects. Thus, we generated group level average time courses reflecting each subject's region of maximum activation. We conducted this analysis both before and after CBA. Additionally, we determined the peak vertex for each subject's four visual quadrant ROIs, i.e. the vertex with the highest t-value. We then defined extended single-subject peak vertex ROIs, which also included the six vertices adjacent to the peak vertex [48]. For each resulting single-subject peak vertex ROI we extracted average time courses (incl. SEM) for all four conditions. We then averaged these timecourses across all subjects. We conducted this analysis both before and after CBA.

Peak vertex distribution maps:

We mapped all peak vertices per visual quadrant before and after CBA and computed the vertex-wise number of peak vertices to estimate the degree of overlap between subjects.

REFERENCES

1 Wandell, B. A., Dumoulin, S. O. & Brewer, A. A. Visual field maps in human cortex. *Neuron* **56**, 366-383, doi:10.1016/j.neuron.2007.10.012 (2007).

2 Corbetta, M. & Shulman, G. L. Control of goal-directed and stimulus-driven attention in the brain. *Nature Reviews Neuroscience* **3**, 201-215, doi:10.1038/nrn755 (2002).

3 Das, M., Bennett, D. M. & Dutton, G. N. Visual attention as an important visual function: an outline of manifestations, diagnosis and management of impaired visual attention. *Br J Ophthalmol* **91**, 1556-1560, doi:10.1136/bjo.2006.104844 (2007).

4 de Haan, B., Bither, M., Brauer, A. & Karnath, H. O. Neural Correlates of Spatial Attention and Target Detection in a Multi-Target Environment. *Cereb Cortex* **25**, 2321-2331, doi:10.1093/cercor/bhu046 (2015).

5 Goodale, M. & Milner, D. One brain - Two visual systems. *Psychologist* **19**, 660-663 (2006).

6 Bergmann, J., Genç, E., Kohler, A., Singer, W. & Pearson, J. Neural Anatomy of Primary Visual Cortex Limits Visual Working Memory. *Cerebral Cortex* **26**, 43-50, doi:10.1093/cercor/bhu168 (2014).

7 Lee, J. *et al.* fMRI evidence of aberrant neural adaptation for objects in schizophrenia and bipolar disorder. *Hum Brain Mapp* **40**, 1608-1617, doi:10.1002/hbm.24472 (2019).

8 Silverstein, S. M. *et al.* An fMRI examination of visual integration in schizophrenia. *J Integr Neurosci* **8**, 175-202, doi:10.1142/s0219635209002113 (2009).

9 Dumoulin, S. O. & Wandell, B. A. Population receptive field estimates in human visual cortex. *Neuroimage* **39**, 647-660, doi:10.1016/j.neuroimage.2007.09.034 (2008).

10 Sereno, M. I. *et al.* Borders of multiple visual areas in humans revealed by functional magnetic resonance imaging. *Science (New York, N.Y.)* **268**, 889-893, doi:10.1126/science.7754376 (1995).

11 Harrison, S. A. & Tong, F. Decoding reveals the contents of visual working memory in early visual areas. *Nature* **458**, 632-635, doi:10.1038/nature07832 (2009).

12 Peters, B., Kaiser, J., Rahm, B. & Bledowski, C. Activity in Human Visual and Parietal Cortex Reveals Object-Based Attention in Working Memory. *The Journal of Neuroscience* **35**, 3360-3369, doi:10.1523/jneurosci.3795-14.2015 (2015).

13 Downing, P. E., Chan, A. W., Peelen, M. V., Dodds, C. M. & Kanwisher, N. Domain specificity in visual cortex. *Cereb Cortex* **16**, 1453-1461, doi:10.1093/cercor/bhj086 (2006).

14 Kanwisher, N., McDermott, J. & Chun, M. M. The fusiform face area: a module in human extrastriate cortex specialized for face perception. *J Neurosci* **17**, 4302-4311, doi:10.1523/jneurosci.17-11-04302.1997 (1997).

15 Brett, M., Johnsrude, I. S. & Owen, A. M. The problem of functional localization in the human brain. *Nat Rev Neurosci* **3**, 243-249, doi:10.1038/nrn756 (2002).
16 Desai, R., Liebenthal, E., Possing, E. T., Waldron, E. & Binder, J. R. Volumetric vs. surface-based alignment for localization of auditory cortex activation. *Neuroimage* **26**, 1019-1029, doi:10.1016/j.neuroimage.2005.03.024 (2005).
17 Dougherty, R. F. *et al.* Visual field representations and locations of visual areas V1/2/3 in human visual cortex. *J Vis* **3**, 586-598, doi:10.1167/3.10.1 (2003).
18 Fischl, B., Sereno, M. I. & Dale, A. M. Cortical surface-based analysis. II: Inflation, flattening, and a surface-based coordinate system. *Neuroimage* **9**, 195-207, doi:10.1006/nimg.1998.0396 (1999).
19 Frost & Goebel. Measuring structural-functional correspondence: spatial variability of specialised brain regions after macro-anatomical alignment. *Neuroimage* **59**, 1369-1381, doi:10.1016/j.neuroimage.2011.08.035 (2012).
20 Frost & Goebel. Functionally informed cortex based alignment: an integrated approach for whole-cortex macro-anatomical and ROI-based functional alignment. *NeuroImage* **83**, 1002-1010, doi:10.1016/j.neuroimage.2013.07.056 (2013).
21 Steinmetz, H., Fürst, G. & Freund, H. J. Variation of perisylvian and calcarine anatomic landmarks within stereotaxic proportional coordinates. *AJNR Am J Neuroradiol* **11**, 1123-1130 (1990).
22 Van Essen, D. C. *et al.* An integrated software suite for surface-based analyses of cerebral cortex. *J Am Med Inform Assoc* **8**, 443-459, doi:10.1136/jamia.2001.0080443 (2001).
23 Zilles, K. *et al.* Quantitative analysis of sulci in the human cerebral cortex: Development, regional heterogeneity, gender difference, asymmetry, intersubject variability and cortical architecture. *Human Brain Mapping* **5**, 218-221, doi:https://doi.org/10.1002/(SICI)1097-0193(1997)5:4<218::AID-HBM2>3.0.CO;2-6 (1997).
24 Bridge, H. Mapping the visual brain: how and why. *Eye (Lond)* **25**, 291-296, doi:10.1038/eye.2010.166 (2011).
25 Fedorenko, E., Hsieh, P. J., Nieto-Castañón, A., Whitfield-Gabrieli, S. & Kanwisher, N. New method for fMRI investigations of language: defining ROIs functionally in individual subjects. *J Neurophysiol* **104**, 1177-1194, doi:10.1152/jn.00032.2010 (2010).
26 Julian, J. B., Fedorenko, E., Webster, J. & Kanwisher, N. An algorithmic method for functionally defining regions of interest in the ventral visual pathway. *NeuroImage* **60**, 2357-2364, doi:10.1016/j.neuroimage.2012.02.055 (2012).
27 Nieto-Castañón, A. & Fedorenko, E. Subject-specific functional localizers increase sensitivity and functional resolution of multi-subject analyses. *Neuroimage* **63**, 1646-1669, doi:10.1016/j.neuroimage.2012.06.065 (2012).
28 Smith, S. M. *et al.* Functional connectomics from resting-state fMRI. *Trends in cognitive sciences* **17**, 666-682, doi:10.1016/j.tics.2013.09.016 (2013).
29 Talairach, J., & Tournoux, P. *Co-planar stereotaxic atlas of the human brain: 3-dimensional proportional system : an approach to cerebral imaging*. (Thieme, 1988).
30 Evans, A. C. *et al.* 3D statistical neuroanatomical models from 305 MRI volumes. *1993 IEEE Conference Record Nuclear Science Symposium and Medical Imaging Conference*, 1813-1817 vol.1813 (1993).
31 Klein, A. *et al.* Evaluation of volume-based and surface-based brain image registration methods. *Neuroimage* **51**, 214-220, doi:10.1016/j.neuroimage.2010.01.091 (2010).
32 Ghosh, S. S. *et al.* Evaluating the validity of volume-based and surface-based brain image registration for developmental cognitive neuroscience studies in children 4 to 11 years of age. *NeuroImage* **53**, 85-93, doi:10.1016/j.neuroimage.2010.05.075 (2010).
33 Nieto-Castanon, A., Ghosh, S. S., Tourville, J. A. & Guenther, F. H. Region of interest based analysis of functional imaging data. *Neuroimage* **19**, 1303-1316, doi:10.1016/s1053-8119(03)00188-5 (2003).

34 Fischl, B., Sereno, M. I., Tootell, R. B. & Dale, A. M. High-resolution intersubject averaging and a coordinate system for the cortical surface. *Hum Brain Mapp* **8**, 272-284, doi:10.1002/(sici)1097-0193(1999)8:4<272::aid-hbm10>3.0.co;2-4 (1999).

35 Anticevic, A. *et al.* Comparing surface-based and volume-based analyses of functional neuroimaging data in patients with schizophrenia. *Neuroimage* **41**, 835-848, doi:10.1016/j.neuroimage.2008.02.052 (2008).

36 Pantazis, D. *et al.* Comparison of landmark-based and automatic methods for cortical surface registration. *Neuroimage* **49**, 2479-2493, doi:10.1016/j.neuroimage.2009.09.027 (2010).

37 Van Essen, D. C. & Drury, H. A. Structural and functional analyses of human cerebral cortex using a surface-based atlas. *J Neurosci* **17**, 7079-7102, doi:10.1523/jneurosci.17-18-07079.1997 (1997).

38 Fischl, B. *et al.* Cortical folding patterns and predicting cytoarchitecture. *Cereb Cortex* **18**, 1973-1980, doi:10.1093/cercor/bhm225 (2008).

39 Hinds, O. P. *et al.* Accurate prediction of V1 location from cortical folds in a surface coordinate system. *NeuroImage* **39**, 1585-1599, doi:10.1016/j.neuroimage.2007.10.033 (2008).

40 Weiner, K. S. *et al.* Defining the most probable location of the parahippocampal place area using cortex-based alignment and cross-validation. *Neuroimage* **170**, 373-384, doi:10.1016/j.neuroimage.2017.04.040 (2018).

41 Rosenke, M., van Hoof, R., van den Hurk, J., Grill-Spector, K. & Goebel, R. A Probabilistic Functional Atlas of Human Occipito-Temporal Visual Cortex. *Cerebral Cortex*, doi:10.1093/cercor/bhaa246 (2020).

42 Huang, T., Chen, X., Jiang, J., Zhen, Z. & Liu, J. A probabilistic atlas of the human motion complex built from large-scale functional localizer data. *Hum Brain Mapp* **40**, 3475-3487, doi:10.1002/hbm.24610 (2019).

43 Di Russo, F., Martínez, A. & Hillyard, S. A. Source analysis of event-related cortical activity during visuo-spatial attention. *Cereb Cortex* **13**, 486-499, doi:10.1093/cercor/13.5.486 (2003).

44 Di Russo, F., Martínez, A., Sereno, M. I., Pitzalis, S. & Hillyard, S. A. Cortical sources of the early components of the visual evoked potential. *Hum Brain Mapp* **15**, 95-111, doi:10.1002/hbm.10010 (2002).

45 Shigihara, Y., Hoshi, H. & Zeki, S. Early visual cortical responses produced by checkerboard pattern stimulation. *NeuroImage* **134**, doi:10.1016/j.neuroimage.2016.03.078 (2016).

46 Kraft, A. *et al.* fMRI localizer technique: efficient acquisition and functional properties of single retinotopic positions in the human visual cortex. *NeuroImage* **28**, 453-463, doi:10.1016/j.neuroimage.2005.05.050 (2005).

47 Bressler, D. W. & Silver, M. A. Spatial attention improves reliability of fMRI retinotopic mapping signals in occipital and parietal cortex. *Neuroimage* **53**, 526-533, doi:10.1016/j.neuroimage.2010.06.063 (2010).

48 Tong, Y. *et al.* Seeking Optimal Region-Of-Interest (ROI) Single-Value Summary Measures for fMRI Studies in Imaging Genetics. *PLoS One* **11**, e0151391, doi:10.1371/journal.pone.0151391 (2016).

49 Anderson, J., Cameron, E. & Levine, M. A method for quantifying visual field inhomogeneities. *Vision Research* **105**, doi:10.1016/j.visres.2014.09.010 (2014).

50 Liu, T., Heeger, D. J. & Carrasco, M. Neural correlates of the visual vertical meridian asymmetry. *J Vis* **6**, 1294-1306, doi:10.1167/6.11.12 (2006).

51 O'Connell, C. *et al.* Structural and functional correlates of visual field asymmetry in the human brain by diffusion kurtosis MRI and functional MRI. *Neuroreport* **27**, 1225-1231, doi:10.1097/wnr.0000000000000682 (2016).

52 Rubin, N., Nakayama, K. & Shapley, R. Enhanced perception of illusory contours in the lower versus upper visual hemifields. *Science* **271**, 651-653, doi:10.1126/science.271.5249.651 (1996).

53 Brodoehl, S., Gaser, C., Dahnke, R., Witte, O. W. & Klingner, C. M. Surface-based analysis increases the specificity of cortical activation patterns and connectivity results. *Scientific Reports* **10**, 5737, doi:10.1038/s41598-020-62832-z (2020).

54 Bullmore, E. & Sporns, O. Complex brain networks: graph theoretical analysis of structural and functional systems. *Nature Reviews Neuroscience* **10**, 186-198, doi:10.1038/nrn2575 (2009).

55 Chen, H., Yao, D. & Liu, Z. A study on asymmetry of spatial visual field by analysis of the fMRI BOLD response. *Brain Topogr* **17**, 39-46, doi:10.1023/b:brat.0000047335.00110.6a (2004).

56 Loughnane, G. M., Shanley, J. P., Lalor, E. C. & O'Connell, R. G. Behavioral and electrophysiological evidence of opposing lateral visuospatial asymmetries in the upper and lower visual fields. *Cortex* **63**, 220-231, doi:10.1016/j.cortex.2014.09.003 (2015).

57 Eickhoff, S. B., Rottschy, C., Kujovic, M., Palomero-Gallagher, N. & Zilles, K. Organizational Principles of Human Visual Cortex Revealed by Receptor Mapping. *Cerebral Cortex* **18**, 2637-2645, doi:10.1093/cercor/bhn024 (2008).

58 Curcio, C. A. & Allen, K. A. Topography of ganglion cells in human retina. *J Comp Neurol* **300**, 5-25, doi:10.1002/cne.903000103 (1990).

59 Silson, E. H., Reynolds, R. C., Kravitz, D. J. & Baker, C. I. Differential Sampling of Visual Space in Ventral and Dorsal Early Visual Cortex. *The Journal of Neuroscience* **38**, 2294-2303, doi:10.1523/jneurosci.2717-17.2018 (2018).

60 Hagler, D. J., Jr. Visual field asymmetries in visual evoked responses. *J Vis* **14**, 13, doi:10.1167/14.14.13 (2014).

61 Schmidtmann, G., Logan, A. J., Kennedy, G. J., Gordon, G. E. & Loffler, G. Distinct lower visual field preference for object shape. *J Vis* **15**, 18, doi:10.1167/15.5.18 (2015).

62 Thomas, N. A. & Elias, L. J. Upper and lower visual field differences in perceptual asymmetries. *Brain Res* **1387**, 108-115, doi:10.1016/j.brainres.2011.02.063 (2011).

63 Zito, G. A., Cazzoli, D., Müri, R. M., Mosimann, U. P. & Nef, T. Behavioral Differences in the Upper and Lower Visual Hemifields in Shape and Motion Perception. *Front Behav Neurosci* **10**, 128-128, doi:10.3389/fnbeh.2016.00128 (2016).

64 Bakroon, A. & Lakshminarayanan, V. Visual function in autism spectrum disorders: a critical review. *Clin Exp Optom* **99**, 297-308, doi:10.1111/cxo.12383 (2016).

65 Butler, P. D. *et al.* Dysfunction of early-stage visual processing in schizophrenia. *Am J Psychiatry* **158**, 1126-1133, doi:10.1176/appi.ajp.158.7.1126 (2001).

66 Butler, P. D., Silverstein, S. M. & Dakin, S. C. Visual perception and its impairment in schizophrenia. *Biol Psychiatry* **64**, 40-47, doi:10.1016/j.biopsych.2008.03.023 (2008).

67 Chen, C. Y. *et al.* Visual spatial attention in children with attention deficit hyperactivity disorder. *Chang Gung Med J* **25**, 514-521 (2002).

68 Hale, T. S. *et al.* Visual Network Asymmetry and Default Mode Network Function in ADHD: An fMRI Study. *Front Psychiatry* **5**, 81, doi:10.3389/fpsyt.2014.00081 (2014).

69 Sanz-Cervera, P., Pastor-Cerezuela, G., González-Sala, F., Tárraga-Mínguez, R. & Fernández-Andrés, M.-I. Sensory Processing in Children with Autism Spectrum Disorder and/or Attention Deficit Hyperactivity Disorder in the Home and Classroom Contexts. *Front Psychol* **8**, 1772-1772, doi:10.3389/fpsyg.2017.01772 (2017).

70 Seymour, R. A., Rippon, G., Gooding-Williams, G., Schoffelen, J. M. & Kessler, K. Dysregulated oscillatory connectivity in the visual system in autism spectrum disorder. *Brain* **142**, 3294-3305, doi:10.1093/brain/awz214 (2019).

71 Shimizu, V. T., Bueno, O. F. & Miranda, M. C. Sensory processing abilities of children with ADHD. *Braz J Phys Ther* **18**, 343-352, doi:10.1590/bjpt-rbf.2014.0043 (2014).

72 Bittner, R. A. *et al.* The When and Where of Working Memory Dysfunction in Early-Onset Schizophrenia-A Functional Magnetic Resonance Imaging Study. *Cereb Cortex* **25**, 2494-2506, doi:10.1093/cercor/bhu050 (2015).

73 Butler, P. D., Thompson, J. L., Seitz, A. R., Deveau, J. & Silverstein, S. M. Visual perceptual remediation for individuals with schizophrenia: Rationale, method, and three case studies. *Psychiatr Rehabil J* **40**, 43-52, doi:10.1037/prj0000212 (2017).

74 Haenschel, C. *et al.* Contribution of impaired early-stage visual processing to working memory dysfunction in adolescents with schizophrenia: a study with event-related potentials and functional magnetic resonance imaging. *Arch Gen Psychiatry* **64**, 1229-1240, doi:10.1001/archpsyc.64.11.1229 (2007).

75 Manoach, D. S. Prefrontal cortex dysfunction during working memory performance in schizophrenia: reconciling discrepant findings. *Schizophr Res* **60**, 285-298, doi:10.1016/s0920-9964(02)00294-3 (2003).

76 French, L. & Paus, T. A FreeSurfer view of the cortical transcriptome generated from the Allen Human Brain Atlas. *Frontiers in Neuroscience* **9**, doi:10.3389/fnins.2015.00323 (2015).

77 Gulban, O. F. *et al.* Improving a probabilistic cytoarchitectonic atlas of auditory cortex using a novel method for inter-individual alignment. *eLife* **9**, e56963, doi:10.7554/eLife.56963 (2020).

78 Hawrylycz, M. J. *et al.* An anatomically comprehensive atlas of the adult human brain transcriptome. *Nature* **489**, 391-399, doi:10.1038/nature11405 (2012).

79 Sabuncu, M. R. *et al.* Function-based Intersubject Alignment of Human Cortical Anatomy. *Cerebral Cortex* **20**, 130-140, doi:10.1093/cercor/bhp085 (2009).

80 Conroy, B. R., Singer, B. D., Guntupalli, J. S., Ramadge, P. J. & Haxby, J. V. Inter-subject alignment of human cortical anatomy using functional connectivity. *NeuroImage* **81**, 400-411, doi:https://doi.org/10.1016/j.neuroimage.2013.05.009 (2013).

81 Glasser, M. F. *et al.* A multi-modal parcellation of human cerebral cortex. *Nature* **536**, 171-178, doi:10.1038/nature18933 (2016).

82 Gulban, O. F. *et al.* Improving a probabilistic cytoarchitectonic atlas of auditory cortex using a novel method for inter-individual alignment. *Elife* **9**, doi:10.7554/eLife.56963 (2020).

83 Oldfield, R. C. The assessment and analysis of handedness: the Edinburgh inventory. *Neuropsychologia* **9**, 97-113, doi:10.1016/0028-3932(71)90067-4 (1971).

84 Goebel, R., Esposito, F. & Formisano, E. Analysis of functional image analysis contest (FIAC) data with brainvoyager QX: From single-subject to cortically aligned group general linear model analysis and self-organizing group independent component analysis. *Hum Brain Mapp* **27**, 392-401, doi:10.1002/hbm.20249 (2006).

85 Sled, J. G., Zijdenbos, A. P. & Evans, A. C. in *Proceedings of the 15th International Conference on Information Processing in Medical Imaging* 459–464 (Springer-Verlag, 1997).

86 Hou, Z., Huang, S., Hu, Q. & Nowinski, W. L. A fast and automatic method to correct intensity inhomogeneity in MR brain images. *Med Image Comput Comput Assist Interv* **9**, 324-331, doi:10.1007/11866763_40 (2006).

87 Kriegeskorte, N. & Goebel, R. An Efficient Algorithm for Topologically Correct Segmentation of the Cortical Sheet in Anatomical MR Volumes. *NeuroImage* **14**, 329-346 (2001).

88 Breman, H. *et al.* in *Biomedical Image Registration.* (eds Žiga Špiclin, Jamie McClelland, Jan Kybic, & Orcun Goksel) 122-130 (Springer International Publishing).

89 Greve, D. N. & Fischl, B. Accurate and robust brain image alignment using boundary-based registration. *Neuroimage* **48**, 63-72, doi:10.1016/j.neuroimage.2009.06.060 (2009).

90 Frost, M. A., Esposito, F. & Goebel, R. Improved correspondence of resting-state networks after macroanatomical alignment. *Hum Brain Mapp* **35**, 673-682, doi:10.1002/hbm.22191 (2014).

91 Wang, L., Mruczek, R. E., Arcaro, M. J. & Kastner, S. Probabilistic Maps of Visual Topography in Human Cortex. *Cereb Cortex* **25**, 3911-3931, doi:10.1093/cercor/bhu277 (2015).

92 Yamamoto, H. *et al.* Inconsistency and uncertainty of the human visual area loci following surface-based registration: Probability and Entropy Maps. *Hum Brain Mapp* **33**, 121-129, doi:10.1002/hbm.21200 (2012).

ACKNOWLEDGEMENTS

The authors are most grateful to Deliah Macht, Christina Raab and Leonie Winkler-Lauble for help with data acquisition. C.V Barnes-Scheufler was supported by a “main doctus” scholarship from The Polytechnic Foundation of Frankfurt am Main. E. Raspor was supported by a Research Grant for Doctoral Programmes in Germany from the German Academic Exchange Service (DAAD).

AUTHOR CONTRIBUTION

All authors made substantial contributions to the conception or design of the work, or the acquisition, analysis, or interpretation of data. AR and RAB acquired funding. RAB, BP, MS and LR designed the experiment. MQ, CVB-S, LR and RAB acquired the data. ER and RG provided analytical tools. MQ and RAB analyzed the data. MQ and RAB undertook the literature searches and wrote the first draft of the manuscript. All authors contributed to and revised the manuscript. All authors read and approved the final manuscript.

DISCLOSURES

The authors have declared that there are no conflicts of interest in relation to the subject of this study.

DATA AVAILABILITY STATEMENT

The data that support the findings of this study are available from the corresponding author upon reasonable request.

FIGURE LEGENDS

Figure 1 – Visual field Localizer Paradigm

The task consisted of flickering, black-and-white colored checkerboards that appeared randomly at homologous positions of the participant's visual quadrant. Only in 25 % of the trials the two centrally located squares changed their color into yellow for 133 ms. Participants were required to press a response box button when noticing that. During the whole task participants were instructed to fixate a black, x-shaped fixation cross presented in the center of the screen. Checkerboards appeared for 2000 ms. The regular inter-stimulus interval was 0 ms. Every 10 to 14 trial the ITI extended to 2000 ms.

Figure 2 – Group analysis of visual quadrants

Surface-based group results (a) before and (b) after CBA (pre-CBA and post-CBA) and averaged time courses. After CBA, group ROIs showed greater spatial consistency and ROIs for the lower visual hemifield were larger in size than ROIs for the upper visual hemifield. Average timecourses (incl. SEM) showed clear position selectivity which was higher after CBA. ROI/graph colors: red = upper left (UL) visual quadrant, orange = lower left (LL) visual quadrant, light-blue = lower right (LR) visual quadrant, dark-blue = upper right (UR) visual quadrant.

Figure 3 – Probability Maps

Probability Maps (a) before and (b) after CBA (pre-CBA and post-CBA) for each visual quadrant. The color code grey-to-white indicates an increase in the probability of overlap. Proba-

bility maps (a) before CBA showed a maximum probability of overlap of up to 50 %. Probability maps (b) after CBA showed a maximum probability of overlap of up to 90 %.

Figure 4 – Probability Difference Maps

Probability difference maps (post-CBA minus pre-CBA). The color code dark-red-to-white indicates an increase of activation overlap. The color code blue-to-green indicate a decrease of activation overlap. Overall, at the center of each ROI the probability of overlap increased by up to forty percent after CBA.

Figure 5 – Average timecourses of visual quadrants

Average timecourses (incl. SEM) of visual quadrants for full single-subject and single-subject extended peak vertex ROIs before and after CBA (pre-CBA and post-CBA). Extended peak-vertex ROIs showed consistently larger BOLD-signal amplitudes. Average timecourses showed clear position selectivity which was unaffected by CBA.

ROI/graph colors: red = upper left (UL) visual quadrant, orange = lower left (LL) visual quadrant, light-blue = lower right (LR) visual quadrant, dark-blue = upper right (UR) visual quadrant. Dashed lines = single subject extended peak-vertex ROIs, solid lines = full single-subject ROIs.

Figure 6 – Peak vertex distribution maps

For each visual quadrant single-subject peak vertices were mapped (a) before and (b) after CBA (pre-CBA and post-CBA) and a vertex-wise number of peak vertices were computed to estimate the degree of overlap. The color code turquoise-to-red indicates an increase in the degree of overlap. After CBA, we observed reduced spatial variability of peak vertex location.

Table 1 – Talairach coordinates

Table 1 depicts the Talairach coordinates of the group ROIs of the corresponding visual quadrants before and after CBA.

Table 1

Region of interest		Number of vertices	Talairach coordinates (in mm)		
			x	y	z
upper right visual quadrant	pre CBA	6	-18	-80	-15
	post CBA	58	-18	-80	-15
upper left visual quadrant	pre CBA	47	24	-75	-14
	post CBA	82	18	-77	-15
lower left visual quadrant	pre CBA	295	-42	-64	5
	post CBA	161	-24	-91	-4
lower right visual quadrant	pre CBA	28	23	-90	3
	post CBA	127	9	-94	-5

Standard Trial
2000 ms
133 ms
133 ms
133 ms
133 ms
133 ms
...
Standard Trial
2000 ms
133 ms
133 ms
133 ms
133 ms
133 ms
...
Target Trial
2000 ms
133 ms
133 ms
133 ms
133 ms
133 ms
...
Standard Trial
2000 ms
133 ms
133 ms
133 ms
133 ms
133 ms
...

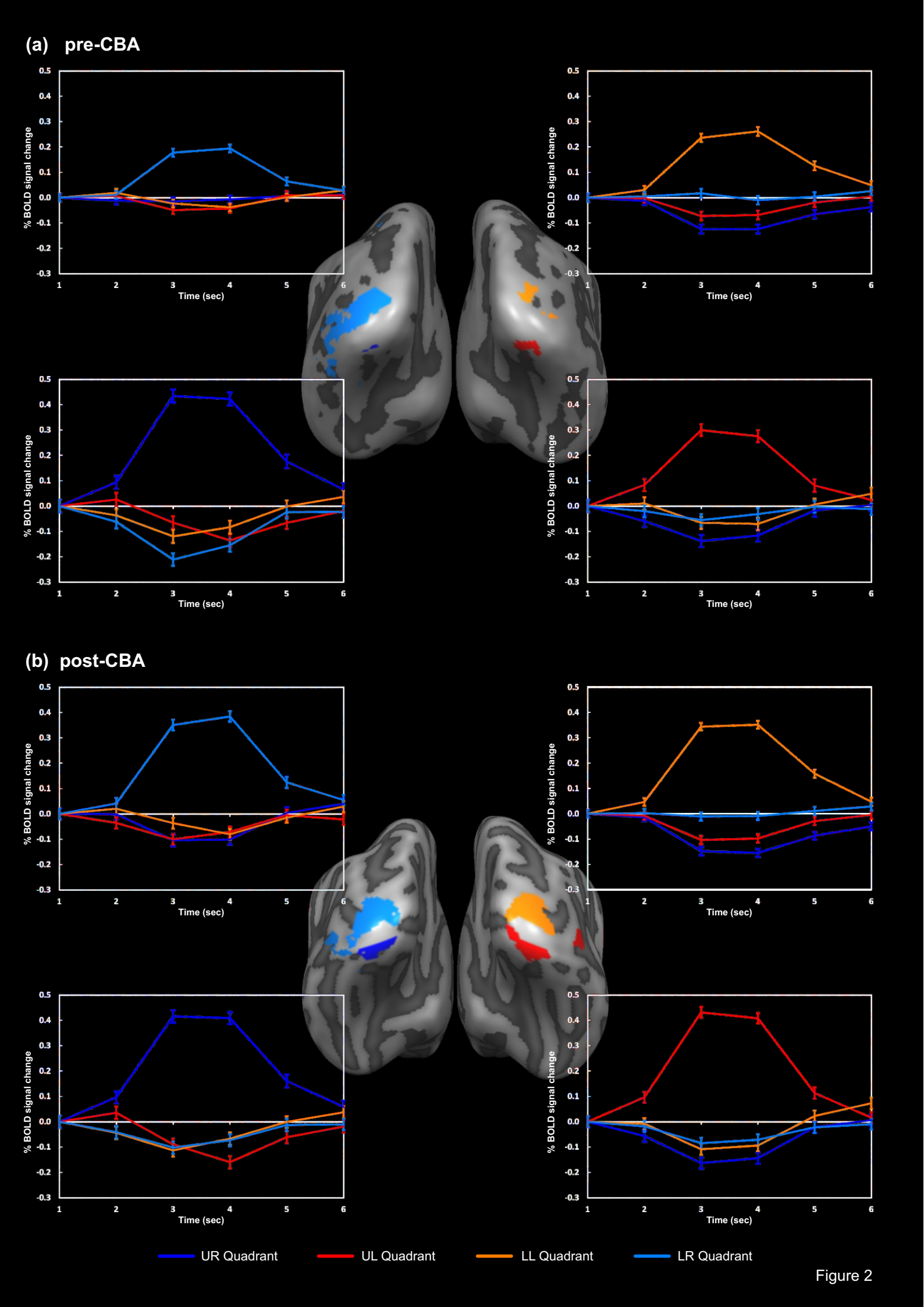
(a) pre-CBA
(b) post-CBA
% BOLD signal change
Time (sec)
UR Quadrant
UL Quadrant
LL Quadrant
LR Quadrant

Figure 2

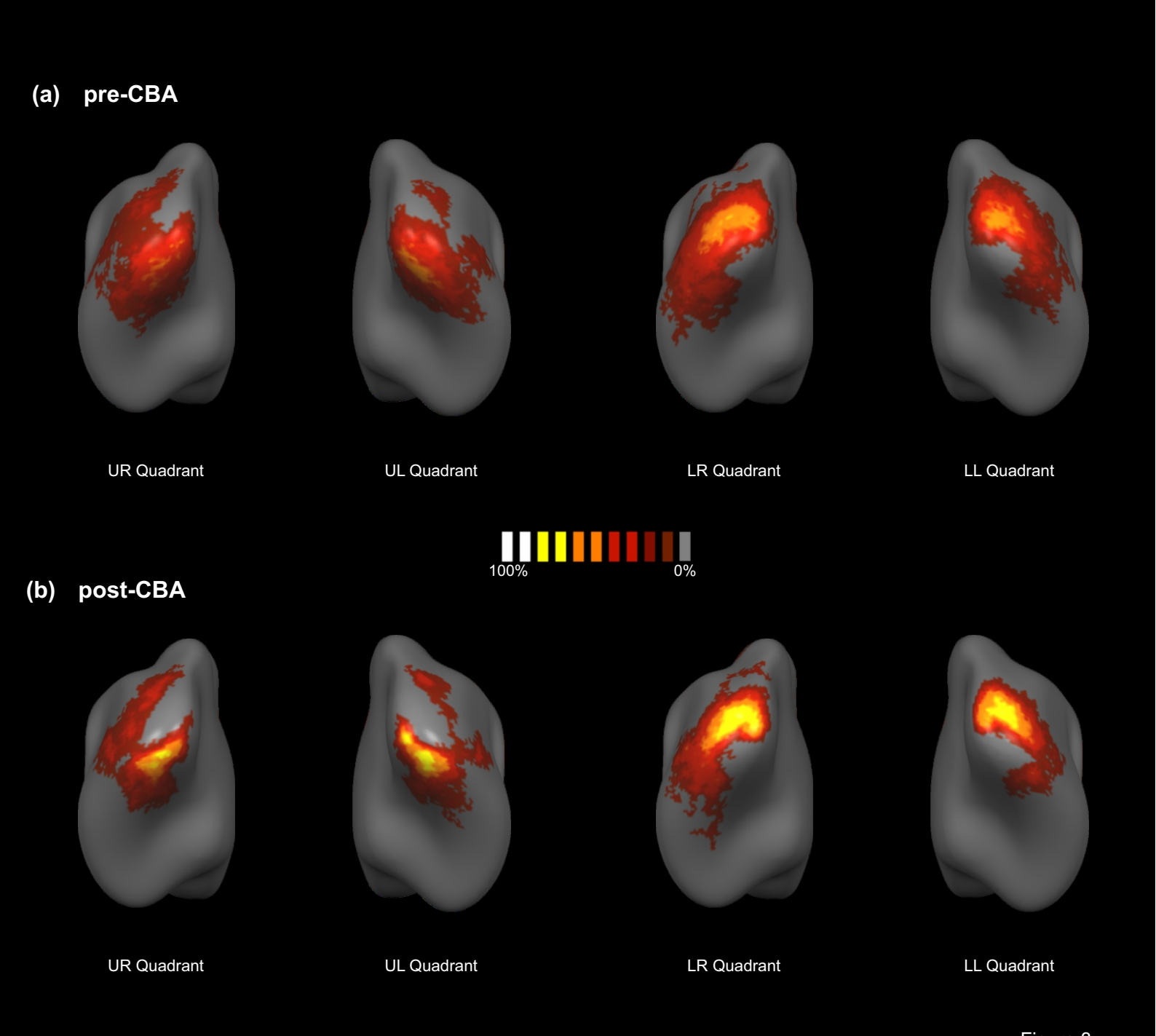
(a) pre-CBA
UR Quadrant
UL Quadrant
LR Quadrant
LL Quadrant
100%
0%
(b) post-CBA
UR Quadrant
UL Quadrant
LR Quadrant
LL Quadrant

Figure 3

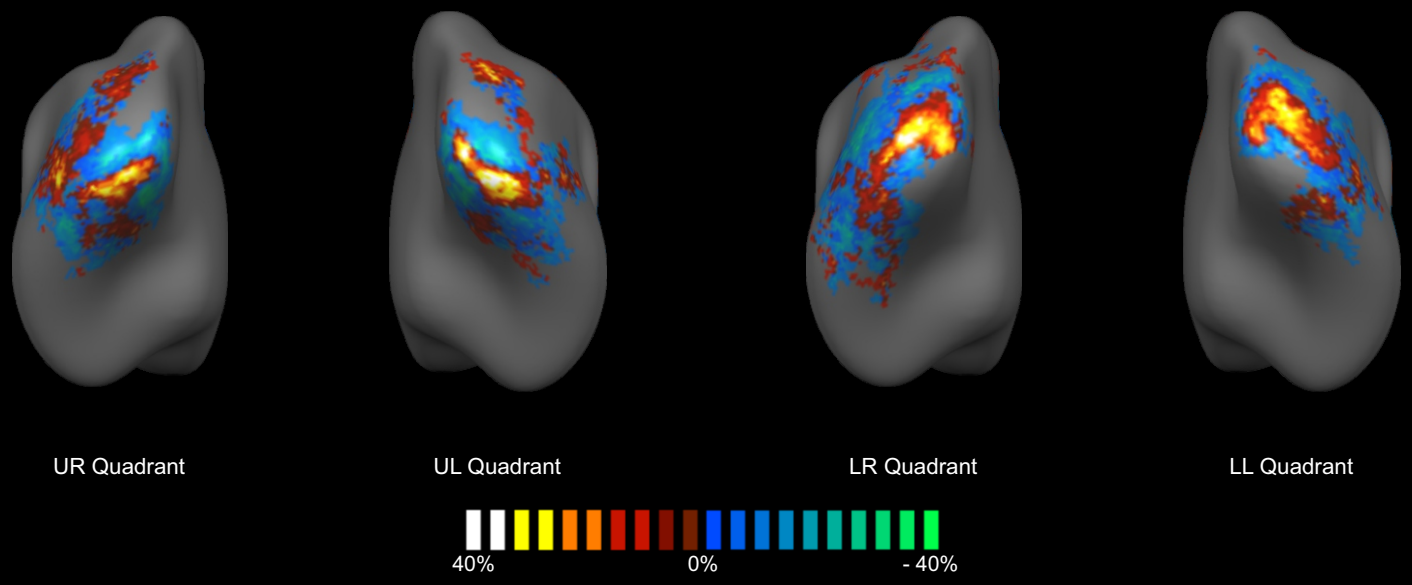

Figure 4

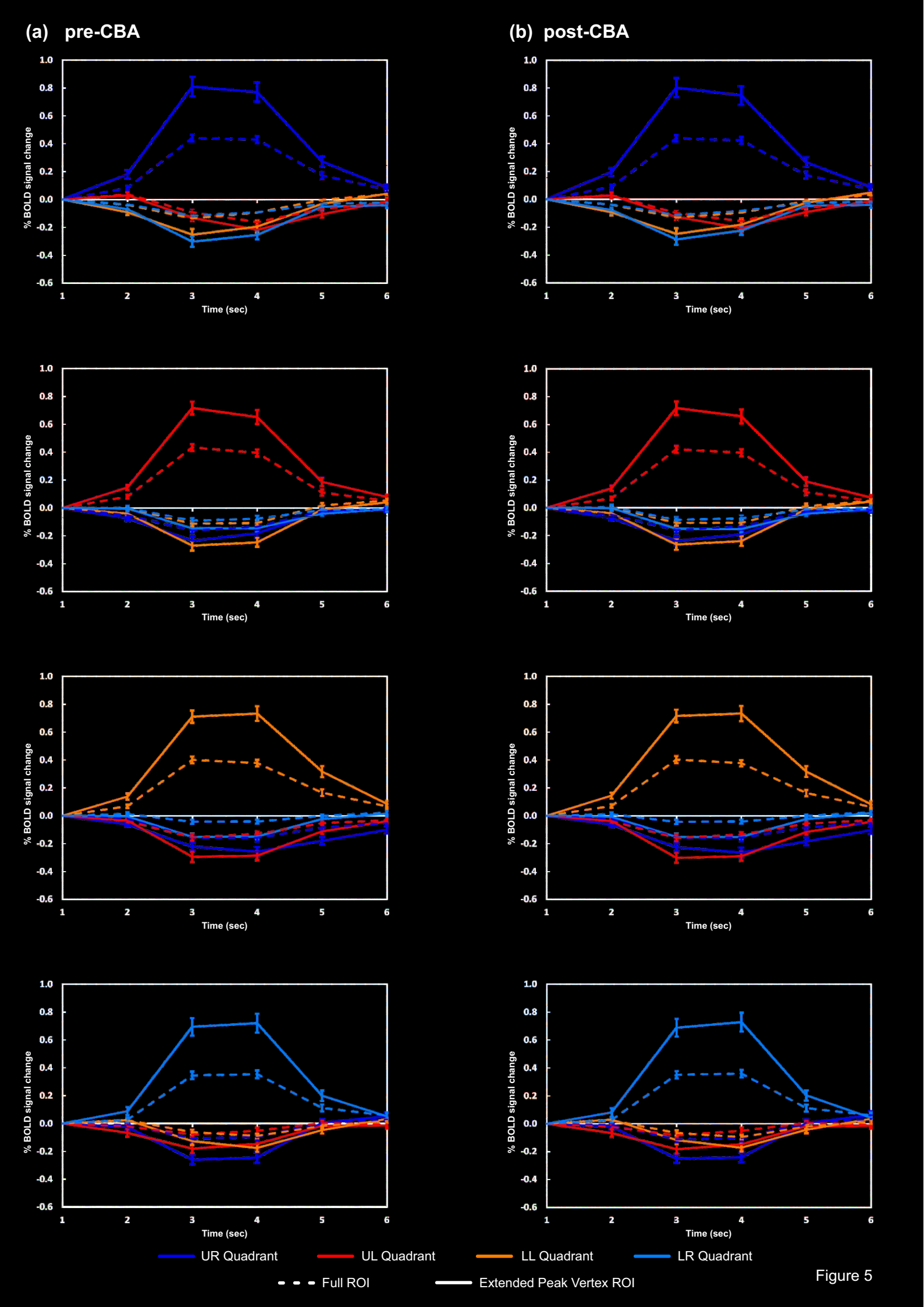
(a) pre-CBA
(b) post-CBA
% BOLD signal change
Time (sec)
UR Quadrant
UL Quadrant
LL Quadrant
LR Quadrant
Full ROI
Extended Peak Vertex ROI

Figure 5

(a) pre-CBA

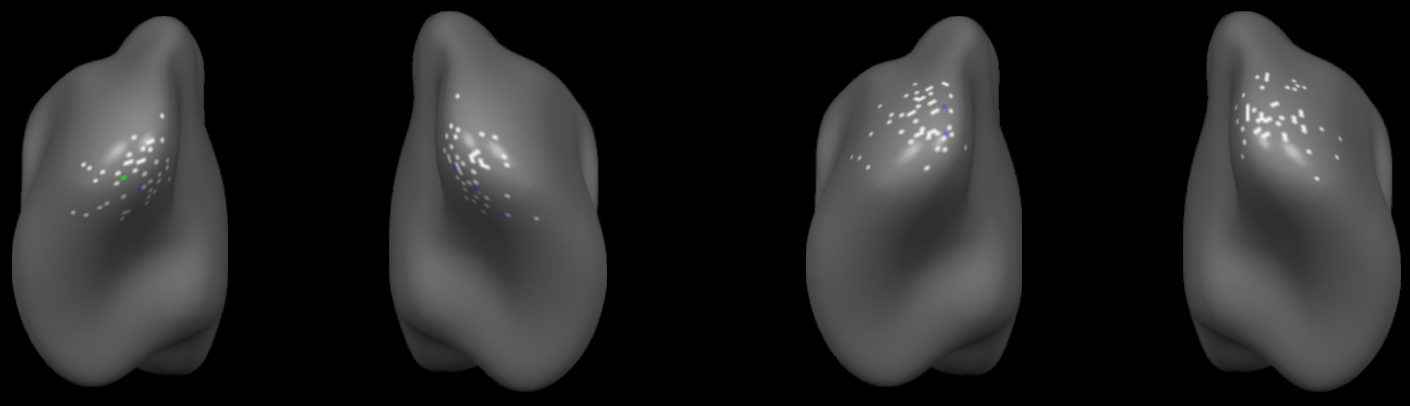

UR Quadrant UL Quadrant LR Quadrant LL Quadrant

(b) post-CBA

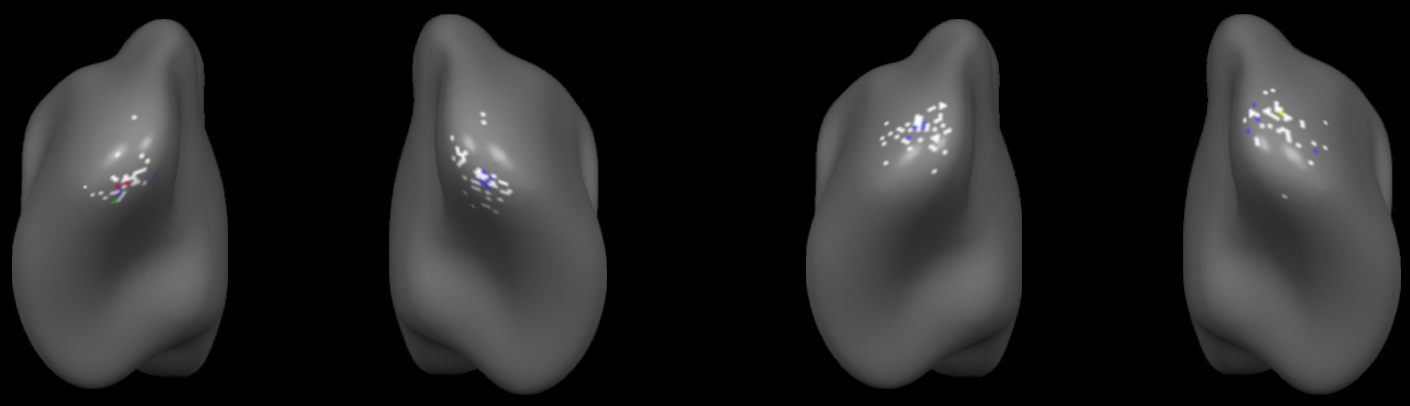

UR Quadrant UL Quadrant LR Quadrant LL Quadrant

Figure 6